inorganics

MDPI

Article

A 4-Methylbenzoylhydrazine Pt(II) Complex Inhibits the Proliferation of Breast Cancer Cells by Regulating the Cell Cycle and Inducing Apoptosis

Huiping Wang, Xianguang Bai *, Yarui Li and Kexin Chen

Department of Basic Medicine, School of Medicine, Pingdingshan University, Pingdingshan 467036, China; 3566@pdsu.edu.cn (H.W.); 211060036@e.pdsu.edu.cn (Y.L.); 211060035@e.pdsu.edu.cn (K.C.)
* Correspondence: xianguangbai@pdsu.edu.cn

Abstract: In this study, a novel 4-methylbenzoylhydrazide·dimethyl sulfoxide·dichloro platinum(II) complex (Pt2) was synthesized and characterized, and its anti-tumor activity and action mechanism were explored. The molecular structure and spatial configuration of the complex were determined using X-ray diffraction. The results obtained using fluorescence spectroscopy demonstrate that this complex can effectively bind to DNA and affect its fluorescence properties. The experimental results show that Pt2 exhibited significant inhibitory effects on a variety of tumor cell lines (MCF-7, HepG-2, NCI-H460, T24, and A549), and its IC50 values were lower than those of cisplatin (DDP), indicating stronger anti-tumor activity. In addition, the complex not only significantly induced the apoptosis of MCF-7 cells but also inhibited cell cycle arrest at the G_2 phase, with the proportion of G_2-phase cells as high as 49.47%. In conclusion, the 4-methylbenzoylhydrazide platinum(II) complex exhibits good anti-tumor activity by inducing apoptosis and inhibiting the cell cycle, providing an important experimental basis for the development of novel platinum-based anti-tumor drugs.

Keywords: Pt(II) complex; anti-tumor activity; apoptosis; cell cycle; DNA binding

check for updates

Academic Editor: Wendell Guerra

Received: 24 April 2025
Revised: 19 May 2025
Accepted: 21 May 2025
Published: 23 May 2025

Citation: Wang, H.; Bai, X.; Li, Y.; Chen, K. A 4-Methylbenzoylhydrazine Pt(II) Complex Inhibits the Proliferation of Breast Cancer Cells by Regulating the Cell Cycle and Inducing Apoptosis. *Inorganics* **2025**, *13*, 177. https://doi.org/10.3390/inorganics13060177

Copyright: © 2025 by the authors. Licensee MDPI, Basel, Switzerland. This article is an open access article distributed under the terms and conditions of the Creative Commons Attribution (CC BY) license (https://creativecommons.org/licenses/by/4.0/).

1. Introduction

Breast cancer stands out as a leading cause of mortality worldwide [1], with its incidence and mortality rates showing varying trends across continents and human development index (HDI) levels [2–4]. Notably, regions with lower HDI levels experience higher mortality-to-incidence ratios, indicating significant disparities in early detection and treatment effectiveness [5–7]. Despite substantial advancements in traditional cancer treatments, such as surgical resection, radiotherapy, and chemotherapy, tumor recurrence and drug resistance persist as formidable challenges in clinical practice [6,8].

In recent years, platinum complexes, as a crucial class of anti-tumor agents, have garnered considerable attention due to their distinctive anti-tumor mechanisms and remarkable therapeutic efficacy [9]. Platinum complexes interact with the DNA in tumor cells to form cross-linking structures, which disrupt DNA replication and transcription [10–12]. This disruption ultimately induces apoptosis and suppresses the proliferation of tumor cells [13–15]. Moreover, platinum complexes can trigger the intracellular oxidative stress response, thereby further augmenting their anti-tumor activity [16]. Hence, the development of platinum complexes characterized by high efficiency and low toxicity holds paramount significance for cancer therapy. Cisplatin (DDP), as the first-generation platinum-based drug, has been extensively applied in the treatment of various solid tumors, including

ovarian cancer, testicular cancer, lung cancer, and head and neck cancer, owing to its broad-spectrum anti-tumor activity [17–21]. Nevertheless, the clinical utilization of DDP is constrained by its severe adverse effects, such as nephrotoxicity, neurotoxicity, and ototoxicity, as well as the issue of drug resistance [19,22]. Inspired by the aim to enhance the efficacy of platinum-based drugs, thousands of cisplatin analogs have been synthesized and screened [23]. However, only a few, such as carboplatin and oxaplatin, have been approved for global use, while nedaplatin, lobaplatin, and heptaplatin have only been approved for use in Asia [24,25].

Notwithstanding the significant progress made in research on platinum drugs, the cis-configuration remains a pivotal feature that enables platinum complexes to exert their anti-tumor activity [26,27]. Therefore, an important research direction in the current study of platinum drugs is to optimize the physical, chemical, and biological properties of platinum complexes by introducing different functional groups and ligands while preserving the cis-configuration [28–30]. Benzoylhydrazine demonstrates potential antitumor activity by inducing cell cycle arrest and promoting tumor cell apoptosis through the mitochondrial pathway [31–33]. Additionally, through the rational design and synthesis of platinum complexes with a cis-configuration, it is possible to further enhance their targeting specificity toward tumor cells and reduce their toxicity to normal cells, thereby enabling more efficient and safer anti-tumor therapy.

Consequently, in this study, a novel platinum complex (Pt2) was synthesized, and its interaction with DNA was investigated using fluorescence spectroscopy. The inhibitory effects of the complex Pt2 on multiple tumor cell lines, including MCF-7, HepG-2, NCI-H460, T24, and A549, were evaluated to assess its anti-tumor activity. The impact of the complex on MCF-7 cells was explored, specifically examining its potential to induce apoptosis and its effect on the cell cycle. The stage of cell cycle arrest was identified, and the proportion of cells in different phases of the cell cycle was determined.

2. Results and Discussion

2.1. Structural Analysis

First, $Pt(DMSO)_2Cl_2$ (Pt1) was synthesized by reacting H_2PtCl_4 with dimethyl sulfoxide (DMSO). Then, the 4-methylbenzoylhydrazide·dimethyl sulfoxide·dichloro platinum(II) complex (Pt2) was prepared via the reaction of benzoylhydrazide with $Pt(DMSO)_2Cl_2$. Their structures were determined using single-crystal X-ray diffraction. The crystal data and structure refinement information are shown in Table 1. The bond length data are presented in Tables S1 and S2, and the bond angle data are listed in Tables S3 and S4.

Table 1. Crystal data and structure refinement for Pt1 and Pt2.

Name	Pt1	Pt2
Empirical formula	$C_4H_{12}Cl_2O_2PtS_2$	$C_{10}H_{16}C_{l2}N_2O_2PtS$
Formula weight	422.254	494.3
Temperature/K	298.15	293(2)
Crystal system	monoclinic	monoclinic
Space group	P21/n	C2/c
a/Å	8.6702(7)	26.8905(15)
b/Å	13.6085(8)	14.0404(6)
c/Å	9.5202(8)	8.7553(5)
α/°	90	90
β/°	106.178(9)	95.597(6)
γ/°	90	90
Volume/$Å^3$	1078.79(15)	3289.8(3)
Z	4	8

Table 1. *Cont.*

Name	Pt1	Pt2
ρ_{calc}g/cm^3	2.6	1.996
μ/mm^{-1}	13.841	8.977
F(000)	781.7	1872
Crystal size/mm^3	0.21 × 0.19 × 0.18	0.18 × 0.19 × 0.19
Radiation	Mo Kα (λ = 0.71073)	Mo Kα (λ = 0.71073)
2θ range for data collection/°	7.46 to 49.98	7.438 to 49.98
Index ranges	$-10 \leq h \leq 10$, $-10 \leq k \leq 17$, $-12 \leq l \leq 7$	$-31 \leq h \leq 31$, $-16 \leq k \leq 16$, $-10 \leq l \leq 10$
Reflections collected	4697	17,409
Independent reflections	1889 [R_{int} = 0.0447, R_{sigma} = 0.0726]	2833 [R_{int} = 0.0599, R_{sigma} = 0.0417]
Data/restraints/parameters	1889/0/104	2833/0/166
Goodness-of-fit on F^2	0.93	1.034
Final R indexes [I $\geq 2\sigma$ (I)]	R_1 = 0.0409, wR_2 = 0.0912	R_1 = 0.0328, wR_2 = 0.0735
Final R indexes [all data]	R_1 = 0.0472, wR_2 = 0.0967	R_1 = 0.0413, wR_2 = 0.0771
Largest diff. peak/hole/e Å^{-3}	3.23/−2.31	0.95/−0.85

The crystal structure of Pt1 is shown in Figure 1, and the crystal packing diagram is shown in Figure S1. Two Cl atoms and two DMSO molecules are coordinated with Pt(II), located at the center. Its crystal system is monoclinic, and the space group is $P2_1/n$. The bond lengths between the Pt(II) ion and Cl1, S2, and S1 are 2.308(3) Å, 2.251(3) Å, and 2.232(2) Å, respectively, and the bond length with Cl2 is 2.316(2) Å, showing slight differences in the lengths of the coordination bonds between Pt(II) and different ligand atoms. In terms of bond angles, S1-Pt1-Cl2 is nearly linear at 178.99(6)°, while S1-Pt1-Cl1 and Cl1-Pt1-Cl2 are 89.31(7)° and 90.13(7)°, respectively, reflecting the special geometric configuration of the Pt(II) center. These structural parameters not only reveal the basic chemical properties of the compound but also lay the foundation for evaluating its thermodynamic stability and potential reactivity.

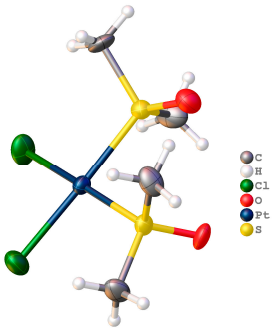

Figure 1. Single-crystal structure of Pt1.

The crystal structure of Pt2 is shown in Figure 2, and the crystal packing diagram is shown in Figure S2. Two Cl atoms, one DMSO molecule, and one benzoylhydrazide molecule are coordinated with the Pt(II) center. Different from $Pt(DMSO)_2Cl_2$, the crystal structure of Pt2 is classified as a monoclinic crystal system, and the space group is C2/c. The unit-cell parameters are a = 26.8905(15) Å, b = 14.0404(6) Å, c = 8.7553(5) Å, α = 90°, β = 95.597(6)°, and γ = 90°. The bond lengths between the Pt(II) ion and S1, Cl2, and Cl1 are 2.2027(16) Å, 2.3271(16) Å, and 2.300(2) Å, respectively, and the bond length with N1 is 2.057(6) Å, revealing the unique relationship of the coordination bond lengths between Pt(II) and different ligand atoms. In terms of bond angles, S1-Pt1-Cl2 is 174.59(9)°, S1-Pt1-Cl1 is 88.77(9)°, and Cl2-Pt1-Cl1 is 87.54(9)°. These bond angle data further depict the geometric configuration of the Pt(II) center. The analysis of bond lengths and angles offers

a fundamental understanding of the compound's structure, contributing to the assessment of its thermal stability and reactivity.

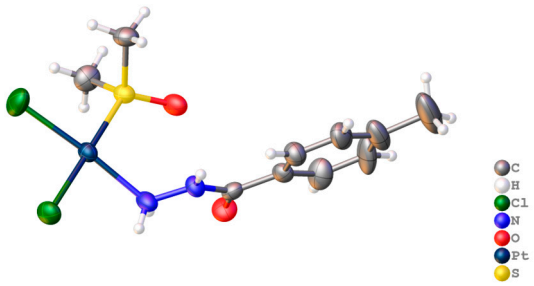

Figure 2. Single-crystal structure of Pt2.

2.2. Binding to DNA

As shown in Figure 3A,B, when the EB-DNA system is excited at 518 nm, there is a fluorescence emission peak at 600 nm. As the concentration of DDP/Pt2 increases, the fluorescence intensity of the system gradually decreases, indicating that fluorescence quenching occurs between DDP/Pt2 and the EB-DNA system. However, the position of the fluorescence emission peak of the system remains unchanged, suggesting that the addition of DDP/Pt2 has no effect on the micro-environment around the EB-DNA system.

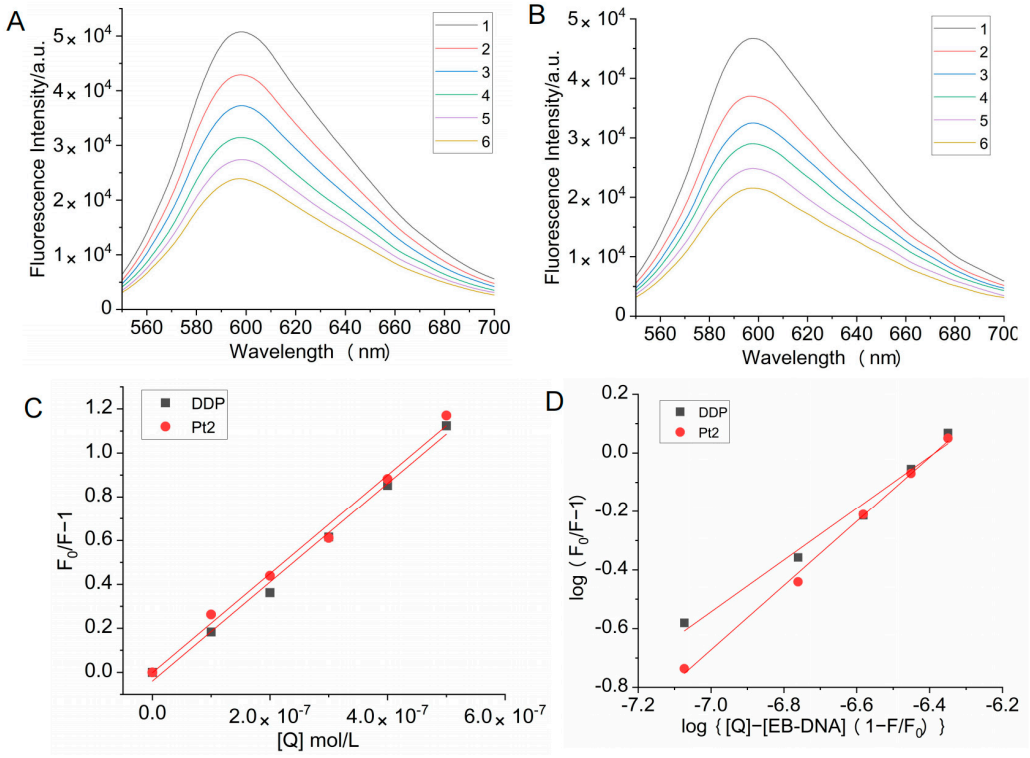

Figure 3. (**A**) The fluorescence-quenching spectrum of EB-DNA by DDP (1–6: 0, 1×10^{-7} mol/L, 2×10^{-7} mol/L, 3×10^{-7} mol/L, 4×10^{-7} mol/L, 5×10^{-7} mol/L) at 310.15 K; (**B**) the fluorescence-quenching spectrum of EB-DNA by Pt2 (1–6: 0, 1×10^{-7} mol/L, 2×10^{-7} mol/L, 3×10^{-7} mol/L, 4×10^{-7} mol/L, 5×10^{-7} mol/L) at 310.15 K; (**C**) the fitting diagram of the Stern–Volmer equation for the fluorescence quenching of EB-DNA by DDP/Pt2 at 310.15 K; (**D**) the fitting diagram of the Lineweaver–Burk equation for the fluorescence quenching of EB-DNA by DDP/Pt2 at 310.15 K.

The relationship between F_0/F and [Q] was plotted to obtain the Stern–Volmer curve for the interaction between DDP/Pt2 and the EB-DNA system at a temperature

of 310.15 K, as shown in Figure 3C. The analysis of this curve reveals that at 310.15 K, the fluorescence-quenching constants of the DDP and Pt2 interactions with the EB-DNA system are 2.2515×10^{16} and 2.2508×10^{16}, respectively. A linear fitting of $\log[(F_0 - F)/F]$ against $n\log\{[Q] - [\text{EB-DNA}](F_0 - F)/F_0\}$ was performed, with the corresponding straight line depicted in Figure 3D. Based on the calculation results of this fitting, the binding constants of DDP and Pt2 with EB-DNA are 4.46×10^5 and 1.01×10^7, respectively, and the numbers of binding sites of DDP and Pt2 with EB-DNA are 0.88 and 1.10, respectively. These data provide crucial quantitative support for exploring the interaction mechanisms of DDP and Pt2 with EB-DNA.

2.3. Anti-Tumor Activity

In this study, the anti-tumor activities of five compounds, namely, K_2PtCl_4, DDP, Pt1, Pt2, and benzoylhydrazide (L), against the tumor cell lines MCF-7, HepG-2, NCI-H460, T24, and A549 were evaluated. The results show that the IC_{50} values of K_2PtCl_4 were greater than 50 for all tested tumor cell lines, and its anti-tumor activity was the weakest among the tested compounds (Table 2). DDP, a commonly used anti-tumor drug in clinical practice, had IC_{50} values of 15.6 ± 0.2 μM, 17.4 ± 0.1 μM, 19.7 ± 0.2 μM, 18.6 ± 0.2 μM, and 20.4 ± 0.3 μM for the MCF-7, HepG-2, NCI-H460, T24, and A549 cell lines, respectively. These results indicate that DDP had a good inhibitory effect on various tumor cell lines, demonstrating strong anti-tumor activity, which is consistent with its performance in clinical applications. The IC_{50} values of Pt1 varied among the different cell lines, ranging from 27.5 ± 0.2 μM (T24 cell line) to 22.1 ± 0.1 μM (HepG-2 cell line). Compared with DDP, its anti-tumor activity was slightly inferior. However, in some cell lines, such as T24 and A549, its activity was higher than that of K_2PtCl_4 and benzoylhydrazide (L), indicating anti-tumor potential. The IC_{50} values of benzoylhydrazide (L) ranged from 26.4 ± 0.3 μM (NCI-H460 cell line) to 48.5 ± 0.4 μM (HepG-2 cell line). Overall, its inhibitory effect on each tumor cell line was relatively limited, and its anti-tumor activity was weak. In comparison with the other tested compounds, it was at a disadvantage. Notably, the IC_{50} values of Pt2 for the MCF-7, HepG-2, NCI-H460, T24, and A549 cell lines were 12.5 ± 0.1 μM, 20.9 ± 0.2 μM, 14.6 ± 0.1 μM, 15.3 ± 0.1 μM, and 16.7 ± 0.1 μM, respectively. The IC_{50} values of this compound were relatively low in most tumor cell lines. Notably, for the MCF-7 cell line, the IC_{50} value was lower than that of DDP. Pt2 exhibits significantly higher potency than DDP and Pt1 across multiple cancer cell lines (e.g., MCF-7, $p < 0.001$). This may be attributed to structural modifications introduced by the benzoylhydrazide ligand, which enhance the complex's lipophilicity (Table S5) and DNA binding affinity, thereby increasing cytotoxicity. This fully demonstrates that Pt2 has strong anti-tumor activity and good application prospects in the field of anti-tumor drug research and development. Further in-depth studies on its mechanism of action and the optimization of the synthesis process are warranted to explore its clinical value.

Table 2. IC_{50} values of K_2PtCl_4, DDP, Pt1, Pt2, and benzoylhydrazide against the cancer cell lines after 48 h.

	IC_{50} (μM)				
	MCF-7	**HepG-2**	**NCI-H460**	**T24**	**A549**
K_2PtCl_4	>50	>50	>50	>50	>50
DDP	15.6 ± 0.2	17.4 ± 0.1	19.7 ± 0.2	18.6 ± 0.2	20.4 ± 0.2
Pt1	28.7 ± 0.3	22.1 ± 0.2	25.9 ± 0.1	27.5 ± 0.2	29.1 ± 0.2
Pt2	12.5 ± 0.1 ***	20.9 ± 0.2 ***	14.6 ± 0.1 ***	15.3 ± 0.1 **	16.7 ± 0.1 ***
Benzoylhydrazide	35.9 ± 0.2	48.5 ± 0.4	26.4 ± 0.3	41.3 ± 0.1	40.8 ± 0.3

Note: Compared to DDP, *** indicates $p < 0.001$, and ** indicates $p < 0.01$.

2.4. Apoptosis Analysis

Figure 4 and Table 3 depict the impact of various compounds on MCF-7 cell apoptosis, with Pt2 demonstrating a particularly potent pro-apoptotic effect. In the experimental setting, upon treatment with cis-Pt2, cell viability plummeted to 61.2%, representing a 35.0% decrease compared to the control group. Notably, compared to the control group, the early apoptosis rate surged to 14.81%, the late apoptosis rate reached 13.159%, and the mortality rate was measured at 7.039%. In stark contrast, other compounds, including DDP, Pt1, and benzoylhydrazide, elicited significantly lower levels of apoptosis and cell death. Specifically, compared to the control group, DDP led to an early apoptosis rate of 11.41% and a late apoptosis rate of 5.739%, while Pt1 resulted in an early apoptosis rate of 4.79% and a late apoptosis rate of 2.779%. In contrast, benzoylhydrazine treatment resulted in 3.71% early apoptosis and 2.539% late apoptosis compared to the control group. In comparison with other platinum complexes reported in previous studies, Pt2 exhibits significantly stronger apoptosis-inducing ability, which may be attributed to the enhanced lipophilicity of its ligand. Lipophilic ligands could potentially improve the cellular uptake efficiency of the drug or directly induce apoptosis by binding to mitochondrial membrane proteins. The high apoptosis rate (31.6%) induced by Pt2 might be associated with the formation of more stable DNA adducts [34–36]. These findings underscore the superiority of cis-Pt2 in inducing apoptosis relative to its counterparts, thereby highlighting its substantial potential in the realm of apoptosis research.

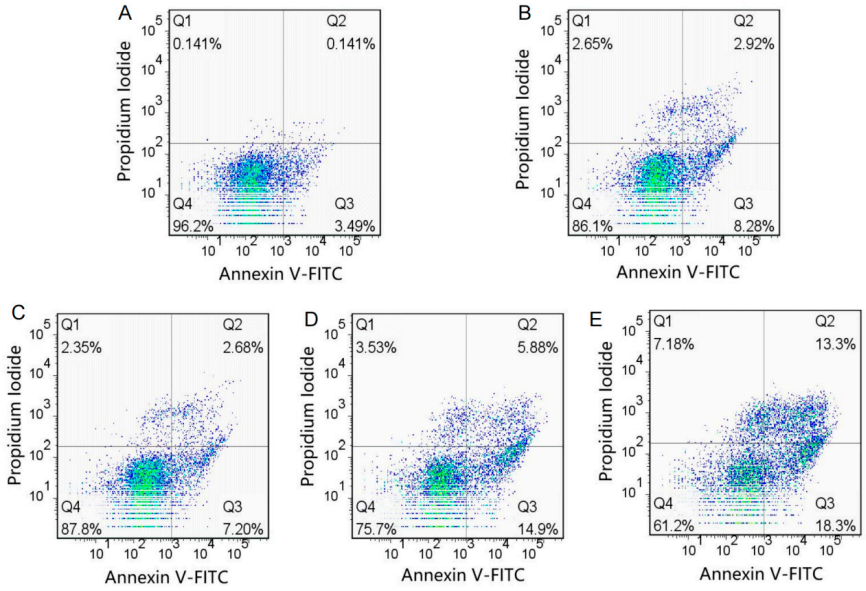

Figure 4. Induction of apoptosis in MCF-7 cells following 24-h treatment with (**A**) the control, (**B**) benzoylhydrazide, (**C**) Pt1, (**D**) DDP, and (**E**) Pt2.

Table 3. Apoptosis rates of breast cancer cells induced by DDP, Pt1, Pt2, and benzoylhydrazine.

	MCF-7 Cell Line			
	Live Cells	**Early Apoptotic Cells**	**Late Apoptotic Cells**	**Necrotic Cells**
Control	96.2%	3.49%	0.141%	0.141%
DDP	75.7%	14.9%	5.88%	3.53%
Pt1	86.1%	8.28%	2.92%	2.65%
Pt2	61.2%	18.3%	13.3%	7.18%
Benzoylhydrazide	87.8%	7.20%	2.68%	2.35%

2.5. Cell Cycle Analysis

Figure 5 and Table 4 illustrate the effects of different compounds on the cell cycle of MCF-7 cells, among which Pt2 shows a remarkable effect in inhibiting the cell cycle. In the experiment, among the cells treated with Pt2, the proportion of cells in the G2 phase was as high as 49.47%, while those in the G1 and S phases were only 33.60% and 16.93%, respectively. This indicates that Pt2 can significantly impede the transition of cells from the G1 phase to the S phase and arrest a large number of cells in the G2 phase. In contrast, other compounds, such as DDP, Pt1, and benzoylhydrazide, had weaker effects on cell cycle arrest. For example, among the cells treated with DDP, the proportion of cells in the G2 phase was 53.50%, but those in the G1 and S phases were 36.84% and 9.66%, respectively. Among the cells treated with Pt1, the proportion of cells in the G2 phase was 41.99%, and those in the G1 and S phases were 44.22% and 13.79%, respectively. Among the cells treated with benzoylhydrazide, the proportion of cells in the G2 phase was 25.79%, and those in the G1 and S phases were 49.46% and 24.76%, respectively. In comparison with previous reports, the G2 phase arrest induced by Pt2 may be associated with the activation of the CHK1/CHK2 pathway triggered by DNA cross-linking damage, a common mechanism of platinum-based compounds. The proportion of cells arrested in the G2 phase by Pt2 (49.47%) is comparable to that of cisplatin (53.50%), indicating that Pt2 exhibits similar efficiency in activating DNA damage response pathways to traditional platinum agents. However, its weaker effect on S-phase cells suggests that Pt2 might be particularly suitable for tumor subtypes that are less sensitive to S-phase targeting [34,37–39]. These data suggest that Pt2 has a particularly outstanding ability to inhibit the cell cycle, demonstrating its significant value in researching cell cycle regulation and potential anticancer mechanisms.

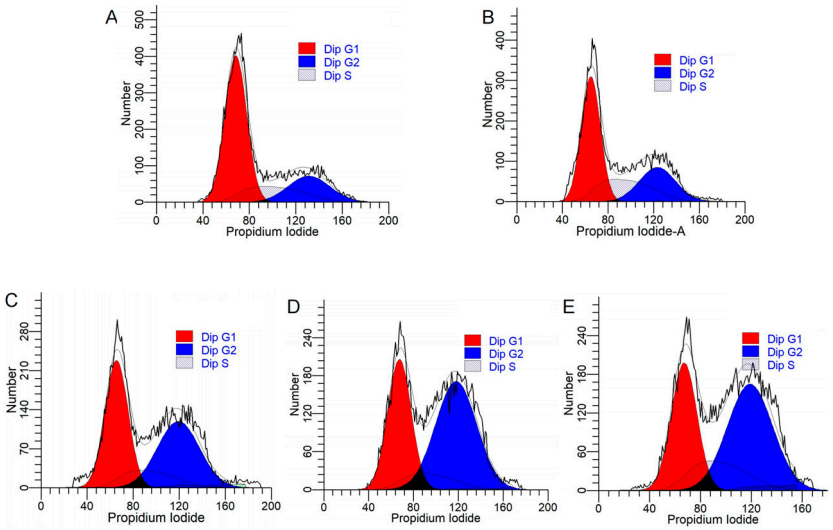

Figure 5. Effects of Bel-7402 treated with (**A**) the control, (**B**) benzoylhydrazide, (**C**) Pt1, (**D**) DDP, and (**E**) Pt2 on the cell cycle.

Table 4. Inhibition rates of DDP, Pt1, Pt2, and benzoylhydrazine on breast cancer cells.

	MCF-7 Cell Line		
	G1	**G2**	**S**
Control	61.07%	20.93%	18.00%
DDP	36.84%	53.50%	9.66%
Pt1	44.22%	41.99%	13.79%
Pt2	33.60%	49.47%	16.93%
Benzoylhydrazide	49.46%	25.79%	24.76%

3. Materials and Methods

3.1. Chemicals

Compounds such as K_2PtCl_4, DMSO, and 4-methylbenzoyl hydrazine were purchased from Shanghai Titan Technology Co., Ltd. (Shanghai, China). All the reagents used were of analytical-grade purity. The cells and culture media were purchased from Wuhan Procell Life Science & Technology Co., Ltd. (Shanghai, China).

3.2. Synthesis of Pt1 and Pt2

Synthesis of Pt1: K_2PtCl_4 (0.1 mmol) was dissolved in DMSO (10 mL), and the solution was heated to 60–70 °C and stirred for 2 h. The generated $Pt(DMSO)_2Cl_2$ was collected via filtration under reduced pressure, washed with cold DMSO, and dried to obtain Pt1. Yield: 79.5%. Anal. calcd (%) for $C_4H_{12}Cl_2O_2PtS_2$: C, 11.38; H, 2.86; O, 7.58. Found: C, 11.31; H, 2.88; O, 7.56. ESI^+ *m*/*z*: calcd for $C_4H_{12}Cl_2O_2PtS_2$, 420.93 [M−H].

Synthesis of Pt2: $Pt(DMSO)_2Cl_2$ (0.1 mmol) was dissolved in ethanol (10 mL), 4-methylbenzoylhydrazine (0.1 mmol) was added, and the mixture was heated and stirred at 60–70 °C for 12 h. After the reaction was completed, the product was collected via filtration under reduced pressure, washed with cold ethanol, and dried to obtain the target complex, Pt2. Yield: 82.5%. Anal. calcd (%) for $C_{10}H_{16}Cl_2N_2O_2PtS$: C, 24.30; H, 3.26; N, 5.67; O, 6.47. Found: C, 24.31; H, 3.24; N, 5.66; O, 6.48. ESI^+ *m*/*z*: calcd for $C_{10}H_{16}Cl_2N_2O_2PtS$, 493.00 [M−H].

3.3. Crystal Structure Determination

The diffraction data of Pt1 and Pt2 were collected on a Bruker D8 Venture X-ray single-crystal diffractometer using Mo Kα radiation (λ = 0.71073 Å) monochromatized by a graphite monochromator with ω and φ scanning modes. The original diffraction data were integrated and reduced using the APEX3 software (version 6) package, and semi-empirical absorption correction was carried out with the SADABS program (Version 2.03). The final crystallographic data completeness reached 98.5%, and the convergence values of R1 and wR2 were 0.0324 and 0.0836 ($I > 2\sigma(I)$), respectively, which confirmed the reliability of the structural analysis.

3.4. Fluorescence Quenching of DNA

At 310.15 K, a pipette was used to transfer 3 mL of a standard calf thymus DNA stock solution with a concentration of 1×10^{-7} mol/L and 300 μL of a standard ethidium bromide solution with a concentration of 1×10^{-7} mol/L to a fluorescence cuvette. The solution was mixed thoroughly, and the fluorescence spectrum of the system without any drugs was measured using a fluorescence spectrophotometer. After taking it out, the EB-DNA system was reconfigured. Then, a pipette was used to sequentially add the DDP or Pt2 solutions with concentrations of 1×10^{-7} mol/L, 2×10^{-7} mol/L, 3×10^{-7} mol/L, 4×10^{-7} mol/L, and 5×10^{-7} mol/L to the system. The samples were placed in the fluorescence spectrophotometer one by one, their fluorescence spectra were measured at wavelengths ranging from 550 nm to 700 nm, and the fluorescence spectra were plotted.

The quenching mechanism was studied by using the Stern–Volmer Equation (1) [40].

$$\frac{F_0}{F} = 1 + K_{SV}[\mathrm{Q}] = 1 + K_{\mathrm{q}}\tau_0[\mathrm{Q}] \quad (1)$$

In the formula, F and F_0 represent the fluorescence intensities of the EB-DNA system in the presence and absence of DDP/Pt2, respectively. [Q] is the concentration of DNA, K_{sv} is the Stern–Volmer quenching constant, K_q is the quenching rate constant, and τ_0 is the

fluorescence lifetime of the fluorophore molecules in the absence of quencher molecules (usually, the fluorescence lifetime of biological macromolecules is approximately 10^{-8} s).

The calculation is carried out by combining the constant Ka and the number of combined bits n through the Lineweaver–Burk Equation (2) [41].

$$\log(F_0/F - 1) = \log K_a + n \log\{[Q] - [EB\text{-}DNA] - (F_0 - F)/F_0\} \quad (2)$$

In the formula, K_a is the binding constant, n is the number of binding sites, and [Q] and [(EB-DNA)] are the total concentrations of DDP/Pt2 and EB-DNA, respectively.

3.5. Anticancer Activity

A total of 180 μL of the cell suspension, adjusted to a density of 5×10^4 cells/mL, was seeded into each well of a 96-well plate. The plate was then incubated at 37 °C in a humidified atmosphere containing 5% CO_2 for 24 h. Subsequently, varying concentrations of the complexes were added to the designated wells. The resulting cell–complex mixtures were further incubated at 37 °C for 48 h in a 5% CO_2 atmosphere. Absorbance values were measured using a microplate reader at dual wavelengths of 570/630 nm. Cytotoxicity was determined by calculating cell viability relative to the negative control group. The final IC_{50} values were calculated using the Bliss method (n = 5). Each experiment was independently repeated three times to ensure data reliability and reproducibility.

3.6. Cell Apoptosis Assay

Cell apoptosis induced by the compounds (10 μM) was detected using an Annexin V-FITC Apoptosis Detection Kit, which combines Annexin V staining with propidium iodide (PI) exclusion. Briefly, cells were adjusted to a density of 1×10^5 cells/mL and incubated with the compounds at 37 °C in a 5% CO_2 atmosphere for 12 h. Following incubation, the MCF-7 cells were resuspended in 100 μL of 1× Annexin V binding buffer. Subsequently, 5 μL each of Annexin V-FITC and PI was added to each sample. The cell suspensions were then incubated at room temperature for 25 min to allow proper staining before being subjected to flow cytometry analysis. This protocol enabled the quantification of early and late apoptotic cells based on their distinct fluorescence profiles.

3.7. Cell Cycle Analysis

MCF-7 cells were cultured in 70 mm dishes until they reached approximately 70% confluence, after which they were treated with the compounds at a defined concentration (10 μM). Following a 24-h treatment period, the cells underwent fluorescence-activated cell sorting (FACS) analysis, as previously described. For cell cycle assessment, the treated cells were first washed, fixed with 75% ethanol, and then rinsed with phosphate-buffered saline (PBS). Subsequently, the cells were stained with propidium iodide (PI) before being analyzed by flow cytometry. For each sample, data from 20,000 individual events were recorded to ensure statistical reliability and comprehensive characterization of the cell cycle distribution.

3.8. Statistical Analysis

All experiments were repeated 3 to 5 times. Student's t-test was used to evaluate the significance of the measured differences. The results are presented as mean ± standard deviation (SD).

4. Conclusions

In this study, Pt2 with a novel structure was successfully synthesized and characterized, and its anti-tumor activity and mechanism of action were systematically evaluated. The

experimental results indicate that this complex exhibits a significant inhibitory effect on various tumor cell lines, and its anti-tumor activity is comparable to that of the traditional platinum-based drug, DDP. Cis-Pt2 can significantly induce cell apoptosis and arrest cells in the G_2 phase, thereby inhibiting the normal progression of the cell cycle. The binding constant (k) of Pt2 to DNA is approximately 22.64-fold higher than DDP, though this difference did not proportionally enhance cytotoxic activity. These findings suggest that Pt2 is a promising candidate for a new type of anti-tumor drug. Its unique chemical structure and remarkable biological activity endow it with broad application prospects in cancer treatment. Future research will further explore its mechanism of action and optimize its synthesis process, with the aim of developing new platinum-based anti-tumor drugs that are more efficient and have lower toxicity.

Supplementary Materials: The following supporting information can be downloaded at https://www.mdpi.com/article/10.3390/inorganics13060177/s1: Table S1: Bond lengths for P1; Table S2: Bond lengths for Pt1; Table S3: Bond angles for Pt2; Table S4: Bond angles for Pt2. Figure S1. Crystal packing diagram of Pt1. Figure S2. Crystal packing diagram of Pt2. Table S5: The logP values of different compounds.

Author Contributions: Conceptualization, X.B.; methodology, H.W.; software, H.W.; validation, H.W.; formal analysis, Y.L.; investigation, K.C.; resources, X.B.; data curation, H.W.; writing—original draft preparation, H.W.; writing—review and editing, X.B.; visualization, Y.L.; supervision, X.B.; project administration, X.B.; funding acquisition, X.B. All authors have read and agreed to the published version of the manuscript.

Funding: This research was funded by the Science and Technology Research Project of Henan Province, grant number 252102311028.

Institutional Review Board Statement: Not applicable.

Informed Consent Statement: Not applicable.

Data Availability Statement: The original contributions presented in this study are included in the article/Supplementary Material. Further inquiries can be directed to the corresponding author.

Conflicts of Interest: The authors declare no conflicts of interest. The funders had no role in the design of the study; in the collection, analyses, or interpretation of data; in the writing of the manuscript; or in the decision to publish the results.

Abbreviations

The following abbreviations are used in this manuscript:

DDP	Cisplatin
Pt2	4-Methylbenzoylhydrazide·dimethyl sulfoxide·dichloro platinum(II) complex
Pt1	$Pt(DMSO)_2Cl_2$
DMSO	Dimethyl sulfoxide
EB	Ethidium bromide
FITC	Fluorescein isothiocyanate

References

1. Cardoso, M.J.; Poortmans, P.; Senkus, E.; Gentilini, O.D.; Houssami, N. Breast cancer highlights from 2023: Knowledge to guide practice and future research. *Breast* **2024**, *74*, 103674. [CrossRef] [PubMed]
2. Tavakoli, B.; Feizi, A.; Zamani-Alavijeh, F.; Shahnazi, H. Factors influencing breast cancer screening practices among women worldwide: A systematic review of observational and qualitative studies. *BMC Womens Health* **2024**, *24*, 268. [CrossRef] [PubMed]
3. Liao, L. Inequality in breast cancer: Global statistics from 2022 to 2050. *Breast* **2025**, *79*, 103851. [CrossRef] [PubMed]
4. Siegel, R.L.; Kratzer, T.B.; Giaquinto, A.N.; Sung, H.; Jemal, A. Cancer statistics, 2025. *CA Cancer J. Clin.* **2025**, *75*, 10–45. [CrossRef]

5. Ehsan, A.N.; Wu, C.A.; Minasian, A.; Bass, M.; Sana, H.; Patel, A.; Pace, L.; Mekary, R.A.; Ranganathan, K. Evaluation of Financial Interventions in Breast Cancer Care Worldwide: A Systematic Review. *Plast. Reconstr. Surg. Glob. Open* **2024**, *12*, e5683. [CrossRef]
6. Meng, G.; Xu, H.; Yang, S.; Chen, F.; Wang, W.; Hu, F.; Zheng, G.; Guo, Y. Bibliometric analysis of worldwide research trends on breast cancer about inflammation. *Front. Oncol.* **2023**, *13*, 1166690. [CrossRef]
7. De Schepper, M.; Vincent-Salomon, A.; Christgen, M.; Van Baelen, K.; Richard, F.; Tsuda, H.; Kurozumi, S.; Brito, M.J.; Cserni, G.; Schnitt, S.; et al. Results of a worldwide survey on the currently used histopathological diagnostic criteria for invasive lobular breast cancer. *Mod. Pathol.* **2022**, *35*, 1812–1820. [CrossRef]
8. da Costa Nunes, G.G.; de Freitas, L.M.; Monte, N.; Gellen, L.P.A.; Santos, A.P.; de Moraes, F.C.A.; da Costa, A.C.A.; de Lima, M.C.; Fernandes, M.R.; Dos Santos, S.E.B.; et al. Genomic Variants and Worldwide Epidemiology of Breast Cancer: A Genome-Wide Association Studies Correlation Analysis. *Genes* **2024**, *15*, 145. [CrossRef]
9. Song, D.; Wang, X.; Zhao, Z.; Yang, R.; Zhang, S.; Guo, Z. Targeting Ribosome Biogenesis for Cancer Therapy with Oral Platinum Complexes. *JACS Au* **2025**, *5*, 73–81. [CrossRef]
10. Tong, K.M.; Toigo, J.; Wolf, M.O. Deep-blue phosphorescence from platinum(ii) bis(acetylide) complexes with sulfur-bridged dipyridyl ligands. *Chem. Sci.* **2025**, *16*, 5948–5956. [CrossRef]
11. Kurochkin, I.Y.; Giricheva, N.I.; Ol'shevskaya, V.A.; Zaitsev, A.V.; Girichev, G.V.; Mitzel, N.W. Geometrical and Electronic Structure of Fluorinated and Non-Fluorinated Platinum(II) Tetraphenylporphyrin Complexes. *Chemphyschem* **2025**, *26*, e202400973. [CrossRef] [PubMed]
12. Jin, S.; He, Y.; Feng, C.; Yuan, J.; Guo, Y.; Guo, Z.; Wang, X. Cellular Discrepancy of Platinum Complexes in Interfering with Mitochondrial DNA. *ACS Cent. Sci.* **2025**, *11*, 393–403. [CrossRef] [PubMed]
13. Bar, S.I.; Schleser, S.W.; Oberhuber, N.; Herrmann, A.; Schlotte, L.; Weber, S.E.; Schobert, R. Trans-[bis(benzimidazol-2-ylidene)dichlorido]platinum(II) complexes with peculiar modes of action and activity against cisplatin-resistant cancer cells. *J. Inorg. Biochem.* **2023**, *238*, 112028. [CrossRef]
14. Velcheva, V.; Hegetschweiler, K.; Momekov, G.; Ivanova, S.; Ugrinov, A.; Morgenstern, B.; Gencheva, G. Platinum(IV) Complexes of the 1,3,5-Triamino Analogue of the Biomolecule Cis-Inositol Designed as Innovative Antineoplastic Drug Candidates. *Pharmaceutics* **2022**, *14*, 2057. [CrossRef]
15. Di Pietro, M.L.; Stagno, C.; Efferth, T.; Omer, E.A.; D'Angelo, V.; Germano, M.P.; Cacciola, A.; De Gaetano, F.; Iraci, N.; Micale, N. Antileukemia Activity and Mechanism of Platinum(II)-Based Metal Complexes. *Molecules* **2022**, *27*, 9000. [CrossRef] [PubMed]
16. Zhang, C.; Kang, T.; Wang, X.; Song, J.; Zhang, J.; Li, G. Stimuli-responsive platinum and ruthenium complexes for lung cancer therapy. *Front. Pharmacol.* **2022**, *13*, 1035217. [CrossRef]
17. Zou, Q.; Chen, Y.; Liu, D.; Du, Q.; Zhang, C.; Mai, Q.; Wang, X.; Lin, X.; Chen, Q.; Wei, M.; et al. Cuproptosis inhibits tumor progression and enhances cisplatin toxicity in ovarian cancer. *FASEB J.* **2025**, *39*, e70484. [CrossRef]
18. Li, S.; Zhang, D.; Li, Y.; Zhou, J.; Chen, J.; Zhang, Y. All-in-one multifunctional tri-block glycopolymers for targeted delivery of cisplatin and cancer chemotherapy. *Colloids Surf. B Biointerfaces* **2025**, *252*, 114639. [CrossRef]
19. Imatsuji, S.; Ujie, Y.; Odake, H.; Imoto, M.; Itoh, S.; Tashiro, E. Cisplatin-induced activation of TGF-beta signaling contributes to drug resistance. *Oncol. Res.* **2023**, *32*, 139–150. [CrossRef]
20. Prasad, R.; Prasad, S.B. Modulatory Effect of Rutin on the Antitumor Activity and Genotoxicity of Cisplatin in Tumor-Bearing Mice. *Adv. Pharm. Bull.* **2021**, *11*, 746–754. [CrossRef]
21. Amini Chermahini, F.; Raeisi, E.; Aazami, M.H.; Mirzaei, A.; Heidarian, E.; Lemoigne, Y. Does Bromelain-Cisplatin Combination Afford In-Vitro Synergistic Anticancer Effects on Human Prostatic Carcinoma Cell Line, PC3? *Galen Med. J.* **2020**, *9*, e1749. [CrossRef] [PubMed]
22. Su, D. MCM7 affects the cisplatin resistance of liver cancer cells and the development of liver cancer by regulating the PI3K/Akt signaling pathway. *Immunopharmacol. Immunotoxicol.* **2022**, *44*, 17–27. [CrossRef]
23. Zhong, T.; Yu, J.; Pan, Y.; Zhang, N.; Qi, Y.; Huang, Y. Recent Advances of Platinum-Based Anticancer Complexes in Combinational Multimodal Therapy. *Adv. Healthc. Mater.* **2023**, *12*, e2300253. [CrossRef] [PubMed]
24. Santos, J.A.V.; Silva, D.; Marques, M.P.M.; Batista de Carvalho, L.A.E. Platinum-based chemotherapy: Trends in organic nanodelivery systems. *Nanoscale* **2024**, *16*, 14640–14686. [CrossRef]
25. Faderin, E.; Iorkula, T.H.; Aworinde, O.R.; Awoyemi, R.F.; Awoyemi, C.T.; Acheampong, E.; Chukwu, J.U.; Agyemang, P.; Onaiwu, G.E.; Ifijen, I.H. Platinum nanoparticles in cancer therapy: Chemotherapeutic enhancement and ROS generation. *Med. Oncol.* **2025**, *42*, 42. [CrossRef]
26. Helleman, J.; Burger, H.; Hamelers, I.H.; Boersma, A.W.; de Kroon, A.I.; Stoter, G.; Nooter, K. Impaired cisplatin influx in an A2780 mutant cell line: Evidence for a putative, cis-configuration-specific, platinum influx transporter. *Cancer Biol. Ther.* **2006**, *5*, 943–949. [CrossRef]
27. Oopkaew, L.; Injongkol, Y.; Kungwan, N.; Rungrotmongkol, T. Theoretical investigation of structure and electronic properties in Cisplatin-citrate complexes. *J. Comput. Chem.* **2025**, *46*, e27511. [CrossRef]

28. Gao, Y.; Huang, Y.; Ren, C.; Xiong, S.; Guo, X.; Zhao, Z.; Guo, L.; Huang, Z. Construction of Cisplatin-18-Crown-6 Complexes Through Supramolecular Chemistry to Improve Solubility, Stability, and Antitumor Activity. *Int. J. Mol. Sci.* **2024**, *25*, 13411. [CrossRef] [PubMed]
29. Dasari, S.; Njiki, S.; Mbemi, A.; Yedjou, C.G.; Tchounwou, P.B. Pharmacological Effects of Cisplatin Combination with Natural Products in Cancer Chemotherapy. *Int. J. Mol. Sci.* **2022**, *23*, 1532. [CrossRef]
30. Li, K.; Li, J.; Li, Z.; Men, L.; Zuo, H.; Gong, X. Cisplatin-based combination therapies: Their efficacy with a focus on ginsenosides co-administration. *Pharmacol. Res.* **2024**, *203*, 107175. [CrossRef]
31. Fu, S.; Liu, J.; Li, C.; Wei, J.; Yue, H.; Yang, A.; Wang, K.; Wu, Y.; Hou, Y.; Zhao, Y. Structure-based drug design, synthesis, and biological evaluation of novel 1,3,5-triazine or pyrimidine derivatives containing benzoyl hydrazine moiety as PI3Kα selective inhibitors. *Bioorg. Chem.* **2023**, *140*, 106738. [CrossRef] [PubMed]
32. Ai, W.; Zuo, Z. Synthesis, optimization and antitumor activity evaluation of sulfonyl benzoyl hydrazide derivatives as novel human LSD1 inhibitors. *Bioorg. Med. Chem. Lett.* **2024**, *114*, 129982. [CrossRef] [PubMed]
33. Li, X.Y.; Liang, J.W.; Mohamed, O.K.; Zhang, T.J.; Lu, G.Q.; Meng, F.H. Design, synthesis and biological evaluation of N-phenyl-(2,4-dihydroxypyrimidine-5-sulfonamido)benzoyl hydrazide derivatives as thymidylate synthase (TS) inhibitors and as potential antitumor drugs. *Eur. J. Med. Chem.* **2018**, *154*, 267–279. [CrossRef]
34. Ciccarone, F.; De Falco, P.; Ciriolo, M.R. Aconitase 2 sensitizes MCF-7 cells to cisplatin eliciting p53-mediated apoptosis in a ROS-dependent manner. *Biochem. Pharmacol.* **2020**, *180*, 114202. [CrossRef]
35. Dasari, S.; Tchounwou, P.B. Cisplatin in cancer therapy: Molecular mechanisms of action. *Eur. J. Pharmacol.* **2014**, *740*, 364–378. [CrossRef]
36. Özdemir, D.; Ağca, C.A. AZD1390, an Ataxia telangiectasia mutated inhibitor, enhances cisplatin mediated apoptosis in breast cancer cells. *Exp. Cell Res.* **2025**, *444*, 114382. [CrossRef] [PubMed]
37. Dasgupta, S.; Kar, K.; Barua, A.; Ghosh, D.; Kabi, B.; Dewan, K.; Chandra, A. A significantly non-toxic novel Cobalt(III) Schiff base complex induces apoptosis via G2-M cell cycle arrest in human breast cancer cell line MCF-7. *Life Sci.* **2022**, *308*, 120963. [CrossRef]
38. Fatehi, R.; Rashedinia, M.; Akbarizadeh, A.R.; Zamani, M.; Firouzabadi, N. Metformin enhances anti-cancer properties of resveratrol in MCF-7 breast cancer cells via induction of apoptosis, autophagy and alteration in cell cycle distribution. *Biochem. Biophys. Res. Commun.* **2023**, *644*, 130–139. [CrossRef]
39. Paramanantham, A.; Kim, M.J.; Jung, E.J.; Kim, H.J.; Chang, S.H.; Jung, J.M.; Hong, S.C.; Shin, S.C.; Kim, G.S.; Lee, W.S. Anthocyanins Isolated from Vitis coignetiae Pulliat Enhances Cisplatin Sensitivity in MCF-7 Human Breast Cancer Cells through Inhibition of Akt and NF-κB Activation. *Molecules* **2020**, *25*, 3623. [CrossRef]
40. Limburg, B. An Extension of the Stern-Volmer Equation for Thermally Activated Delayed Fluorescence (TADF) Photocatalysts. *J. Phys. Chem. Lett.* **2024**, *15*, 10495–10499. [CrossRef]
41. Ngo, A.N.; Murowchick, J.; Gounev, A.D.; Gounev, T.K.; Youan, B.C. Physico-chemistry and Cytotoxicity of Tenofovir-Loaded Acid Phosphatase-Responsive Chitosan Nanoparticles. *AAPS PharmSciTech* **2023**, *24*, 143. [CrossRef] [PubMed]

Disclaimer/Publisher's Note: The statements, opinions and data contained in all publications are solely those of the individual author(s) and contributor(s) and not of MDPI and/or the editor(s). MDPI and/or the editor(s) disclaim responsibility for any injury to people or property resulting from any ideas, methods, instructions or products referred to in the content.